INFERENCE OF STRESS AND TEXTURE FROM ANGULAR DEPENDENCE OF ULTRASONIC PLATE MODE VELOCITIES

R.B. Thompson, J.F. Smith, and S.S. Lee
Iowa State University
Ames, Iowa 50011

The theory for the angular dependence of the ultrasonic wave velocity in a symmetry plane of an orthorhombic, stressed material is presented. The two waves having polarizations in this plane are shown to have velocities which can be estimated from measurements of the SH_0 and S_0 guided modes of a thin plate: the relationship being exact for the SH_0 mode and requiring a 10% correction for the S_0 mode at long wavelength. It is then shown how stress and texture can be independently inferred from various features of the angular dependence of these two velocities. From the SH_0 data, the ability to determine the directions and differences in magnitudes of principal stresses is described and supported by experimental data on several materials. From a combination of the SH_0 and S_0 data, a procedure is proposed for determining the coefficients W_{400}, W_{420}, and W_{440} of an expansion of the crystallite orientation distribution function in terms of generalized Legendre functions. Possible applications in process control are indicated.

INTRODUCTION

Successful process control requires the nondestructive characterization of a number of structural properties. Included are hardness, grain size, ductility, strength, preferred orientation, and stress. This paper discusses techniques whereby significant information related to the latter two quantities in rolled plate can be inferred from the angular dependence of the velocity of ultrasonic waves propagating in the plane of the plate.

THEORY OF THE ANGULAR DEPENDENCE OF ULTRASONIC VELOCITY

Consider a rolled plate and a coordinate system in which the 1, 2, and 3 axes coincide, respectively, with the rolling direction, the transverse direction, and the thickness direction, as shown in figure 1. Assume that the material can be represented as an elastic continuum with orthorhombic symmetry, and imagine that a biaxial stress is present in the plane of the plate with principal values σ_a and σ_b and orientation angle Ω as shown in figure 2. The velocity of ultrasonic waves propa-

*This work was performed for the U.S. Department of Energy, Office of Basic Energy Sciences, Division of Materials Sciences, under contract No. W-7405-Eng-82.

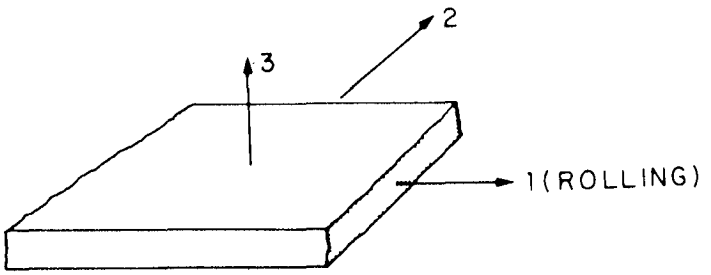

Fig. 1. Coordinate system.

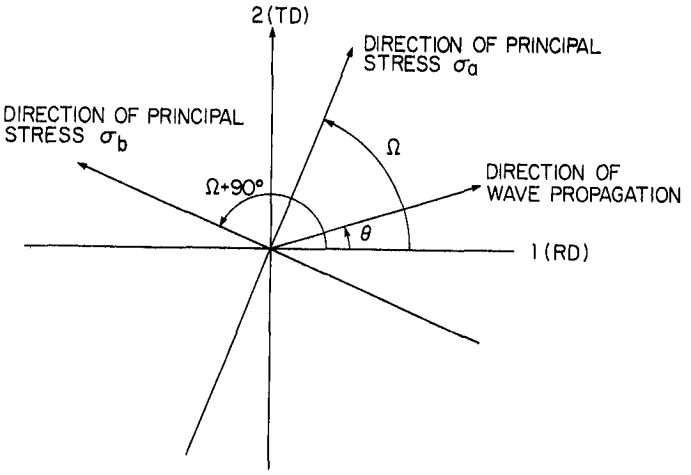

Fig. 2. Orientation of stress and wave propagation direction.

gating in the plane of the plate, i.e. guided modes of the plate, must be obtained by solving the nonlinear, anisotropic equations of dynamic elasticity subject to the stress free boundary conditions on the two surfaces of the plate. The formidable job can be simplified by first neglecting the plate surfaces and treating plane wave propagation in an unbounded medium. Using an analysis, the solutions for the longitudinal and transverse modes, to second order in the elastic anisotropy, are found to be of the form

$$\rho V_L^2 = \bar{C}_L + T + \frac{\bar{\alpha}}{2}\bar{C}_L \cos 2\theta - \frac{\bar{\beta}}{2}\bar{C}_T (1-\cos 4\theta) - \frac{\bar{\beta}^2 \bar{C}_T^2}{4(\bar{C}_L-\bar{C}_T)}\left[(1-\cos 4\theta)^2 - 2(1-\cos 4\theta)\right] + \frac{\bar{\alpha}^2}{32}\frac{\bar{C}_L^2}{(\bar{C}_L-\bar{C}_T)}\left[1-\cos 4\theta\right] + \frac{\bar{\alpha\beta}}{4}\frac{\bar{C}_L\bar{C}_T}{(\bar{C}_L-\bar{C}_T)}\left[(1-\cos 4\theta)(\cos 2\theta)\right] + (\bar{C}_{16}+\bar{C}_{26})\sin 2\theta + \frac{1}{2}(\bar{C}_{16}-\bar{C}_{26})\sin 4\theta \quad (1)$$

$$\rho V_T^2 = \bar{C}_T + T + \frac{\bar{\beta}}{2}\bar{C}_T\,(1-\cos 4\theta) + \frac{\bar{\beta}^2\,\bar{C}_T^{\,2}}{4\,(\bar{C}_L-\bar{C}_T)}\,[(1-\cos 4\theta)^2 - 2\,(1-\cos 4\theta)]$$

$$- \frac{\bar{\alpha}^2}{32}\frac{\bar{C}_L^{\,2}}{(\bar{C}_L-\bar{C}_T)}\,[1-\cos 4\theta] - \frac{\bar{\alpha}\bar{\beta}}{4}\frac{\bar{C}_L\bar{C}_T}{(\bar{C}_L-\bar{C}_T)}\,(1-\cos 4\theta)\,(\cos 2\theta) \qquad (2)$$

$$- \frac{1}{2}\,(\bar{C}_{16} - \bar{C}_{26})\,\sin 4\theta$$

Here ρ is density, $V_{L,T}$ is the wave velocity of longitudinal and transverse waves, θ is the angle of propagation with respect to the 1-direction, $\bar{C}_T = \bar{C}_{66}$, $\bar{C}_L = (\bar{C}_{11} + \bar{C}_{22})/2$, $\bar{\alpha} = (\bar{C}_{11} - \bar{C}_{22})/C_L$, $\bar{\beta} = [(C_L - \bar{C}_{12})/2 - \bar{C}_T]/\bar{C}_T$. The latter two parameters are measures of longitudinal and shear wave velocity anisotropies, respectively. In addition,

$$T = (\sigma_a + \sigma_b)/2 + [(\sigma_a - \sigma_b)/2]\cos 2\,(\Omega - \theta) \qquad (3)$$

where σ_a and σ_b are the principal stresses with the former acting along an axis inclined at an angle Ω with respect to the 1-direction. In the absence of stress, the $\bar{C}_{ij}$ are equal to the anisotropic elastic stiffnesses of the orthorhombic continuum, for which $\bar{C}_{16} = \bar{C}_{26} = 0$. Hence there are nine independent values (ref. 1). When stress is present, there will be small shifts in the values of these nine constants (ref. 2). If $\Omega \neq 0$ the constant $\bar{C}_{16}$ and $\bar{C}_{26}$ will no longer vanish due to the lowering of the effective symmetry of the problem from orthorhombic to triclinic.

The solution V_L corresponds to a quasi-longitudinal wave which is polarized in the 1-2 plane, while the solution V_T corresponds to a quasi-transverse wave polarized in the same plane. A third solution, polarized along the 3-direction, also exists which will not be discussed here.

The relationship of these plane wave solutions for an unbounded medium will next be related to wave propagation in a plate. Consider first the shear wave solution given by equation (2). Examination of the full solution shows that all stress components vanish on planes Z = constant. Hence the plane wave results are also exact solutions in the plate geometry. Since they are uninfluenced by the position of the plate faces, they are non-dispersive. This solution is known as the SH_o mode of the plate (ref. 3).

The plane waves whose velocities are given by equation (1) are not exact solutions in the plate geometry since the dynamic stress component σ_{33} does not vanish for these solutions. However, a simple approximation exists when the frequency is sufficiently low that the wavelength is large with respect to the plate thickness. In isotropic, linear elasticity, the fundamental, symmetric Lamb mode ref. 3), S_o, is known to propagate with a velocity of $V_{S_o} = V_{L_o}\left[1-\left(\frac{\nu}{1-\nu}\right)^2\right]^{1/2}$ in the low frequency limit. Here V_{L_o} is the plane wave longitudinal velocity and ν is Poisson's ratio. For a Poisson's ratio of 0.3, $V_{S_o}/V_{L_o} = 0.90$.

In an orthorhombic material, this relationship generalizes to

$$V_{S_o} = V_{L_o}(1-C_{13}^{\,2}/C_{11}C_{33})^{1/2} \qquad (4)$$

for propagation along the "i" symmetry axis. Thus the correction relating the plate to plane wave velocities will depend on direction. The correction is the order of 10% as noted above, and it depends on elastic constants which only vary by a few percent in modestly textured materials. Hence, in many cases, the angular dependence of the correction may be negligible and its isotropic value can be used. This point will be discussed further in the second section following.

As an experimental test of equation (2), consider the plot of $\Delta V/V$ versus for θ for 6061 Al in figure 3 (ref. 4). In the upper plot, $\sigma_a = \sigma_b = 0$ and the data are fitted well by the first and third term on the right hand side of equation (2). When $\sigma_a \neq 0$ and $\Omega = 0$, the results shown in the lower plot were obtained. Here the theory includes the first three terms. $\overline{C}_T$ was shifted slightly to fit the zero degree data, σ_a was determined from load cell readings, and $\overline{\beta}$ was held equal to the unstressed value. Although some minor differences between theory and experiment are observed, the agreement is believed to be quite good. This is consistent with the theoretical expectation that the remaining omitted terms vary as a higher order in the anisotropy.

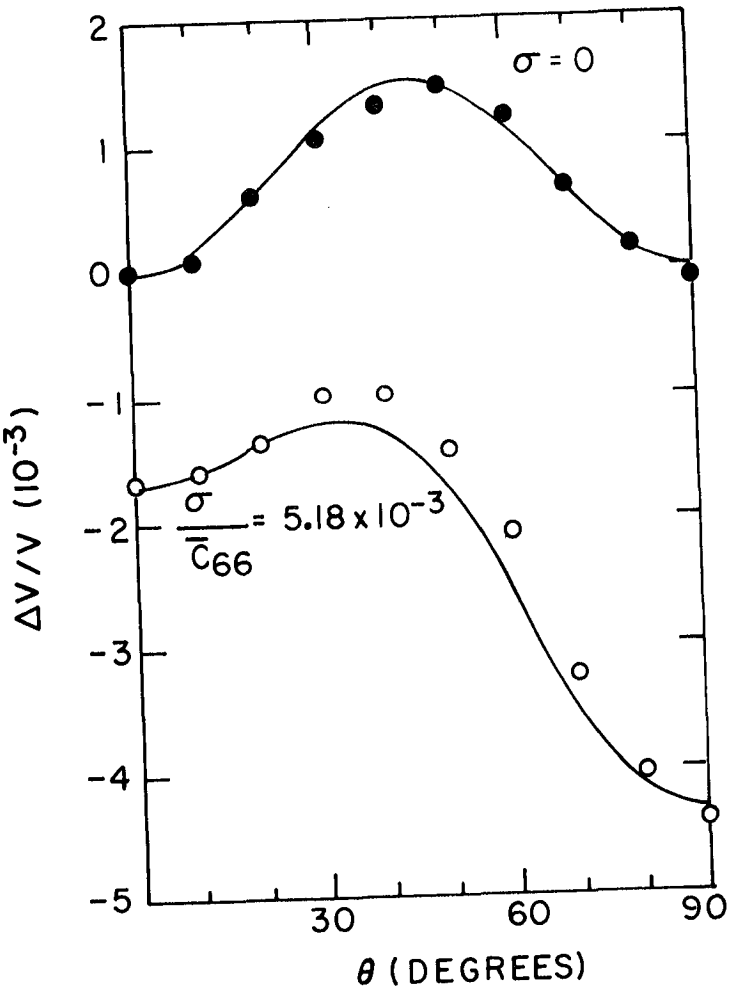

Fig. 3. Comparison of predicted and applied stress in 6061-T6 aluminum when stress is not parallel to material symmetry axes. Experimental configuration is shown in the inset and the method of comparison is described in the text.

DETERMINATION OF STRESS

Stress may be determined from measurements of the shear wave velocity as predicted by equation (2). As the results are discussed in detail elsewhere (refs. 4-8), only a brief summary will be given. Consider first the expression for T in equation (3). Note that no material constants influence the dependence of T on σ_a and σ_b. Thus, if the contributions of the terms following T in equation (2) could be suppressed, the difference in principle stresses, $\sigma_a - \sigma_b$, could be determined from measurements of the angular dependence of V_T. This can be accomplished by noting that all but one of those terms has four-fold symmetry. Thus, if one measures $V_T(\theta)$ and $V_T(\theta + 90°)$ and takes the difference in ρV^2, it follows that

$$[V_T(\theta) - V_T(\theta + 90°)]/\bar{V}_T = \left(\frac{1}{2\rho\bar{V}_T^2}\right)\left[(\sigma_a - \sigma_b)\cos 2(\Omega - \theta) - \frac{\bar{\alpha}\,\bar{\beta}\,\bar{C}_L\,\bar{C}_T}{4(\bar{C}_L - \bar{C}_T)}(\cos 2\theta - \cos 6\theta)\right]. \tag{5}$$

where $\bar{V}_T \triangleq [V(\theta) + V_T(\theta + 90°)]/2$. For small anisotropies, one can approximate $\rho\bar{V}_T^2$ by $\bar{C}_T$ for further simplification.

The final term in equation (5) is second order in the elastic anisotropy. In cases in which it is negligible, the principal stress difference may be deduced by varying θ until the magnitude of the left hand side of equation (5) is maximized and setting that value equal to $(\sigma_a - \sigma_b)/2\ C_T$. As an example, figure 4 presents a comparison of measured and predicted stress in a second 6061-T6 aluminum plate having an unstressed SH_o wave velocity anisotropy of 0.5%, as distinct from the 0.15% anisotropy of the first sample shown in figure 3. The stress was applied at 45° with respect to the rolling direction, $\Omega = 45°$. The maximum value of velocity shift between the θ and θ+90° directions was observed to occur when $\theta = 45°$, and a plot of predicted stress versus applied stress (not shown) closely followed the ideal, unity slope line (ref. 8). However, that was not a critical test of the smallness of the final term in equation (5) since $\cos 2\theta = \cos 6\theta = 0$ for $\theta = 45°$. Hence the measurement direction was then changed to $\theta = 15°$ so that the final term would no longer vanish identically. In the plot shown in figure 4, the predicted stress was deduced on the basis of inserting the known values of $\Omega = 45°$, $\theta = 15°$ into equation (5) and neglecting the final term. The excellent agreement is consistent with the postulated small value of this second order anisotropy term, at least in the particular aluminum sample studied.

If the anisotropy term is not small, a procedure is still available for removing its influence on the data. Note that equation (5) contains only one term with a 6θ-angular variation, which has as its coefficient the second order material anisotropy parameters. Determination of that coefficient from the value of the 6θ term in a Fourier series representation of $[V_T(\theta) - V_T(\theta + 90°)]$ should allow the entire anisotropy term to be subtracted from the data. The previously described procedure could then be applied to the corrected data.

Other than the example illustrated in figure 4, a detailed experimental study of this proposed procedure for non-parallel principal stress and material symmetry axes has not yet been completed. However, when $\Omega = 0$, a number of samples have been studied (refs. 4, 6-8). Figure 5 presents, as an example, the results in a 304

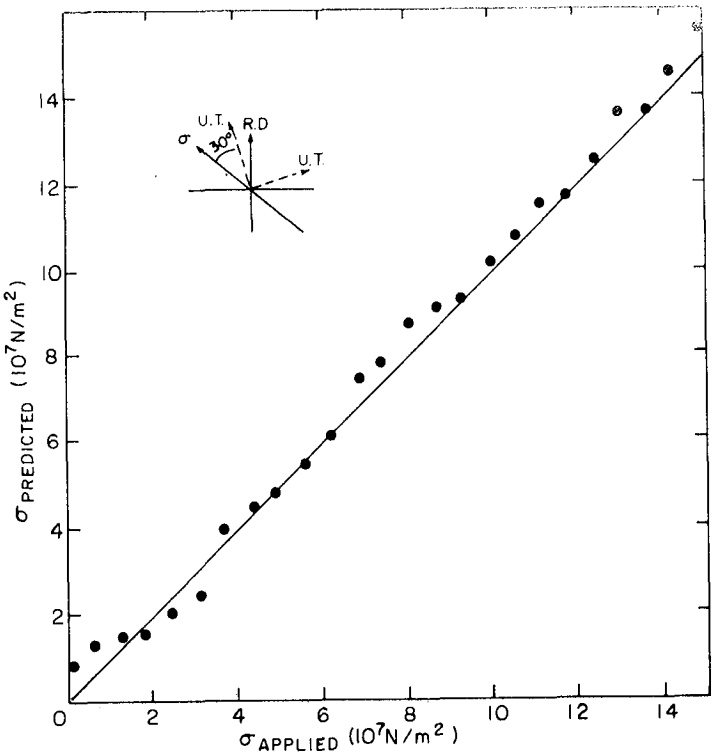

Fig. 4. Comparison of predicted and applied stress in 6061-T6 aluminum when stress is not parallel to material symmetry axes. Experimental configuration is shown in the inset and the method of comparison is described in the text

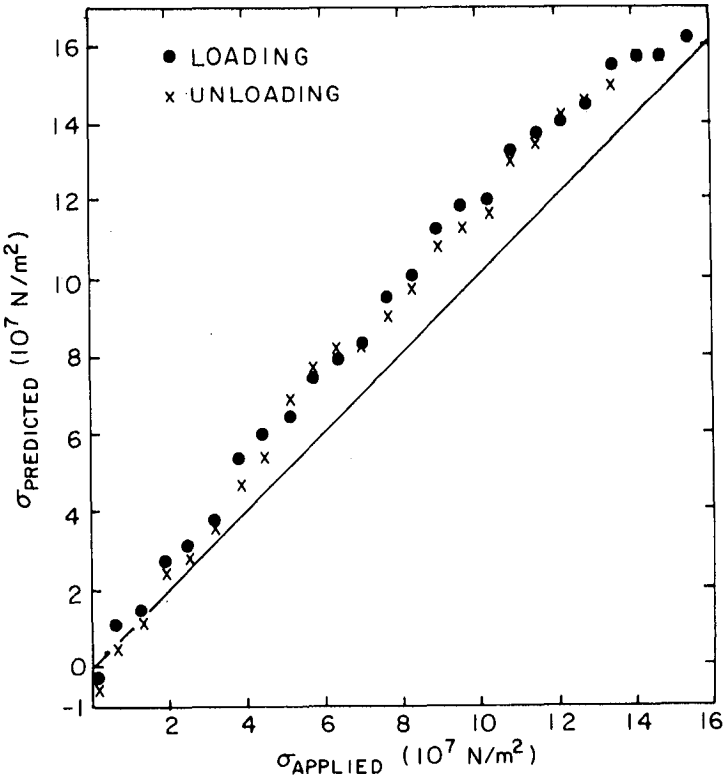

Fig. 5. Comparison of predicted and applied stress in 6061-T6 aluminum plate.

stainless steel sample having an unstressed SH_0 velocity anisotropy of 1.5%. Agreement of predicted and applied stress is excellent. Similar results have been obtained on 6061 aluminum, commercially pure copper, and 1100 aluminum plate. In the latter case, tensile plastic deformation of 0.6% did not destroy the agreement. In an additional sample of titanium (ref. 8), errors occurred due to the absence of the assumed orthorhombic symmetry in the unstressed state.

DETERMINATION OF TEXTURE

In the measurement of stress, the effects of texture were suppressed by comparing the SH_0 velocities measured before and after rotating the propagation direction by 90°. However, those suppressed terms may be used to directly determine important parameters of the preferred orientation. The possibility of inferring preferred orientation from measurements of the anisotropies of the elastic constants or sound velocities has been demonstrated by several authors (refs. 9-11). The present discussion differs from the prior work in two regards. First, the nondestructive measurement of the velocity anisotropy can be made with couplant free EMAT transducers (ref. 12). Hence operation in an on-line, process control mode at room or elevated temperatures is possible (ref. 13). Second, using relationships recently reported by Sayers and Allen (ref. 2) the velocity anisotropies can be directly related to coefficients of the expansion of the crystallite orientation distribution function (CODF) in terms of generalized Legendre functions (refs. 13, 14).

For a material with unknown stress orientations, the procedure would be as follows. First the techniques described in the above section should be employed to determine the principal stress directions and differences. This allows the angular variation of the term T to be removed from equations (1) and (2). If one restricts attention to the velocities measured at 0°, 45°, and 90°, one finds

$$\bar{C}_T + (\sigma_a+\sigma_b)/2 = \rho V_T^2(0°) - [(\sigma_a-\sigma_b)/2] \cos 2\Omega \tag{6a}$$

$$\bar{C}_T + (\sigma_a+\sigma_b)/2 + \bar{\beta}\bar{C}_T - \frac{\bar{\alpha}^2}{16}\frac{\bar{C}_L^2}{(\bar{C}_L - \bar{C}_T)} = \rho V_T^2(45°) - [(\sigma_a-\sigma_b)/2] \sin 2\Omega \tag{6b}$$

$$\bar{C}_T + (\sigma_a+\sigma_b)/2 = \rho V_T^2(90°) + [(\sigma_a-\sigma_b)/2] \cos 2\Omega \tag{6c}$$

$$\bar{C}_L + (\sigma_a+\sigma_b)/2 + \frac{\bar{\alpha}}{2}\bar{C}_L = \rho V_L^2(0°) - [(\sigma_a-\sigma_b)/2] \cos 2\Omega \tag{6d}$$

$$\bar{C}_L + (\sigma_a+\sigma_b)/2 - \bar{\beta}\bar{C}_T + \frac{\bar{\alpha}^2}{16}\frac{\bar{C}_L}{(\bar{C}_L - \bar{C}_T)} + \bar{C}_{16} + \bar{C}_{26} = \rho V_L^2(45°) - [(\sigma_a-\sigma_b)/2] \sin 2\Omega \tag{6e}$$

$$\bar{C}_L + (\sigma_a+\sigma_b)/2 - \frac{\bar{\alpha}}{2}\bar{C}_L = \rho V_L^2(90°) + [(\sigma_a-\sigma_b)/2] \cos 2\Omega \tag{6f}$$

In each of these equations, the experimentally observable velocities, and the inferred principal stress orientations and differences are placed on the right-hand side and can be considered as known quantities.

After noting that equations (6a) and (6c) are not independent because of the relationship between $[V_T^2(0°)-V_T^2(90°)]$ and $[\sigma_a-\sigma_b]$, one concludes that there are five equations in the six unknowns, $\overline{C}_T$, $\overline{C}_L$, $(\sigma_a+\sigma_b)$, and $(\overline{C}_{16}+\overline{C}_{26})$. Hence, a rigorous solution is not possible, and some further approximations will be required. Since $\overline{C}_{16}$ and $\overline{C}_{26}$ appear only in equation (6e) and are not of primary interest, this equation will be dropped leaving four equations in five unknowns. By elementary manipulations it can be concluded that

$$\overline{C}_L + (\sigma_a+\sigma_b)/2 = \rho[V_L^2(0°) + V_L^2(90°)]/2 \tag{7a}$$

$$\overline{\alpha}\,\overline{C}_L = \rho[V_L^2(0°) - V_L^2(90°)] - (\sigma_a-\sigma_b)\cos 2\Omega \tag{7b}$$

$$\overline{C}_T + (\sigma_a+\sigma_b)/2 = \rho[V_T^2(0°) + V_T^2(90°)]/2 \tag{7c}$$

$$\overline{\beta}\,\overline{C}_T - \frac{\overline{\alpha}^2}{16}\frac{\overline{C}_L^2}{(\overline{C}_L - \overline{C}_T)} = \rho\,[V_T^2(45°) - V_T^2(0°)] + [\sigma_a-\sigma_b)/2]\,[\cos 2\Omega - \sin 2\Omega] \tag{7d}$$

The stress terms on the left-hand side of equations (7a) and (7c) will generally be small with respect to $\overline{C}_L$ and $\overline{C}_T$ and can be neglected. However, those on the right-hand side must be retained as they appear in conjunction with the difference of two numbers, which could be of comparable magnitude. It should also be noted that, in general, $\overline{\alpha}$, $\overline{\beta}$, $\overline{C}_T$, and $\overline{C}_L$ are themselves weakly modified by stress through the stress dependence of the $\overline{C}_{ij}$. In general, these are small effects and will be neglected hereafter. In many applications, determination of texture would be done in the unstressed state and the above considerations are unnecessary. Finally, the term proportional to $\overline{\alpha}^2$ in equation (7d) can be dropped for modest textures. The result is the simplified system

$$C_L \cong \rho\,[V_L^2(0°) + V_L^2(90°)]/2 \tag{8a}$$

$$C_T \cong \rho\,[V_T^2(0°) + V_T^2(90°)]/2 \tag{8b}$$

$$\alpha C_L \cong \rho\,[V_L^2(0°) - V_L^2(90°)] - (\sigma_a-\sigma_b)\cos 2\Omega \tag{8c}$$

$$\beta C_T \cong \rho\,[V_T^2(45°)-V_T^2(0°)]+[(\sigma_a-\sigma_b)/2]\,[\cos 2\Omega-\sin 2\Omega], \tag{8d}$$

which can readily be solved for C_L, C_T, α, and β.

The coefficients of the CODF expansion are finally obtained from the relation ship between α, β, C_L, and C_T and the coefficients $W_{\ell mn}$ as defined by the CODF expansion (refs. 2, 14)

$$W(\xi,\psi,\Phi) = \sum_{\ell=o}^{\infty}\sum_{m=-\ell}^{\ell}\sum_{n=-\ell}^{\ell} W_{\ell mn} Z(\xi) e^{-im\psi} e^{-in\Phi} \tag{9}$$

where W is the CODF expressed in terms of the Euler angles ξ, ψ, Φ and $Z_{\ell mn}$ are generalized Legendre functions. Sayers and Allen have derived the relationship between the ultrasonic velocities and the $W_{\ell mn}$ using the method of Voigt to compute polycrystalline averages (ref. 2). Following Bunge (ref. 15), they conclude that only three independent coefficients enter in the calculation of elastic constants for cubic crystallites, W_{400}, W_{420}, and W_{440}. One additional coefficient, W_{000}, is determined by normalization. In texture analysis, the preferred direction in equation (9) is generally taken to be the rolling direction, which leads to a different axis identification than that shown in figure 1 and used throughout the rest of this paper. After rotation to such a system, as employed by Sayers and Allen (ref. 2), in which the 1, 2, and 3 axes correspond respectively to the normal, transverse, and rolling directions, one concludes

$$\rho[V_L^2(0°) + V_L^2(90°)]/2 = C_{11}° - 2C° \left[\frac{1}{5} - \frac{11}{35}\sqrt{2}\,\pi^2 W_{400} - \frac{4}{35}\sqrt{5}\,\pi^2 W_{420} - \frac{2}{35}\sqrt{35}\,\pi^2 W_{440}\right] \tag{10a}$$

$$\rho[V_T^2(0°) + V_T^2(90°)]/2 = C_{44}° + C° \left[\frac{1}{5} - \frac{16}{35}\sqrt{2}\,\pi^2 W_{400} - \frac{16}{35}\sqrt{5}\,\pi^2 W_{420}\right] \tag{10b}$$

$$\rho[V_L^2(0°) - V_L^2(90°)] - (\sigma_a - \sigma_b)\cos 2\Omega = 4C° \left[\frac{5}{35}\sqrt{2}\pi^2 W_{400} - \frac{4}{35}\sqrt{5}\,\pi^2 W_{420} - \frac{2}{35}\sqrt{35}\,\pi^2 W_{440}\right] \tag{10c}$$

$$\rho[V_T^2(45°) - V_T^2(0°)] + [(\sigma_a - \sigma_b)/2]\,[\cos 2\Omega - \sin 2\Omega] = C°\left[\sqrt{2}\,\pi^2 W_{400} + \frac{28}{35}\sqrt{5}\,\pi^2 W_{420} + \frac{2}{35}\sqrt{35}\,\pi^2 W_{440}\right] \tag{10d}$$

where $C_{11}°$, $C_{44}°$, and $C_{12}°$ are single crystal elastic constants and $C° = C_{11}° - C_{12}° - 2C_{44}°$. The $W_{\ell mo}$ are defined in a coordinate system with the 3-axis along the rolling direction, in contrast to the elastic constants appearing in previous equations in this paper. However, the experimental observables on the left hand side of equation (10) are unambiguous.

This constitutes an overdetermined system, since there are four equations in the three unknowns, $W_{\ell mo}$. Either experimental error or inaccuracies in the Voigt averaging scheme would render an exact solution of all equations impossible. A detailed analysis of the most stable data reduction scheme has not yet been conducted. However, it can be speculated that equations (10c) and (10d) should be weighed heavily since the experimental quantities are relative velocities, rather than the absolute velocities appearing in equations (10a) and (10b). It is also likely that equation (10b) will prove more accurate than equation (10a) because no correction of plate to plane wave velocities is required. Whereas such a correction may be quite satisfactory for relative measurements, it may be inadequate for absolute measurements. Thus a first attempt at reduction to practice might involve disregarding equation (10a) and solving the three remaining systems simultaneously.

As a check, one should use the computed $W_{\ell mn}$ values to test the accuracy of the isotropic approximation to the correction relating the velocities V_{L_o} and V_{S_o} as given by equation (4). For larger textures, an iterative solution might be required in which first estimates of the W's are used to recalculate the velocities $V_{L_o}(0°)$ and $V_{L_o}(90°)$ using equation (4) and the polycrystalline averaged elastic constant expressions (ref. 2)

$$C_{13} = C_{12}^{\circ} + C^{\circ} \left[\frac{1}{5} - \frac{16}{35}\sqrt{2}\,\pi^2 \left(W_{400} - \sqrt{5/2}\,W_{420}\right)\right] \tag{11a}$$

$$C_{23} = C_{12}^{\circ} + C^{\circ} \left[\frac{1}{5} + \frac{4}{35}\sqrt{2}\,\pi^2 \left(W_{400} - \sqrt{70}\,W_{440}\right)\right] \tag{11b}$$

Again, a mixed notation has been used in this equation. The elastic constants appearing on the left hand side of equation (11) are defined in the coordinated system of figure 1. The W_{4mo} are defined after Sayers and Allen (ref. 2) as discussed above. As expected, the deviations from the isotropic assumptions will become greater when either the single crystal anisotropy, C°, or the degree of preferred orientation, as indicated by the W_{4mo}, are large.

The above describes one approach to deduce the coefficients of the CODF from the angular dependence of the SH_o and S_o plate mode velocities. Smith et al. (ref. 16) have discussed a closely related approach in which the velocities of higher order, horizontally polarized plate modes, SH_n, are measured and used to predict the anisotropic elastic constants. The experimental parameters of that approach could be related to the $W_{\ell mn}$ using arguments similar to the one presented above.

CONCLUDING REMARKS

It has been shown that measurements of the angular dependence of the SH_o and S_o ultrasonic modes of a plate are influenced by both stress and texture. Data reduction schemes are presented for making independent estimates of a) the orientations and difference of in-plane principal stresses and b) the coefficients W_{400}, W_{420}, and W_{440} of the CODF expansion. Since the data can be obtained with couplant free, EMAT probes, there appears to be a high potential for in-line process control applications (ref. 17). Figure 6 sketches the required measurements. Since the use

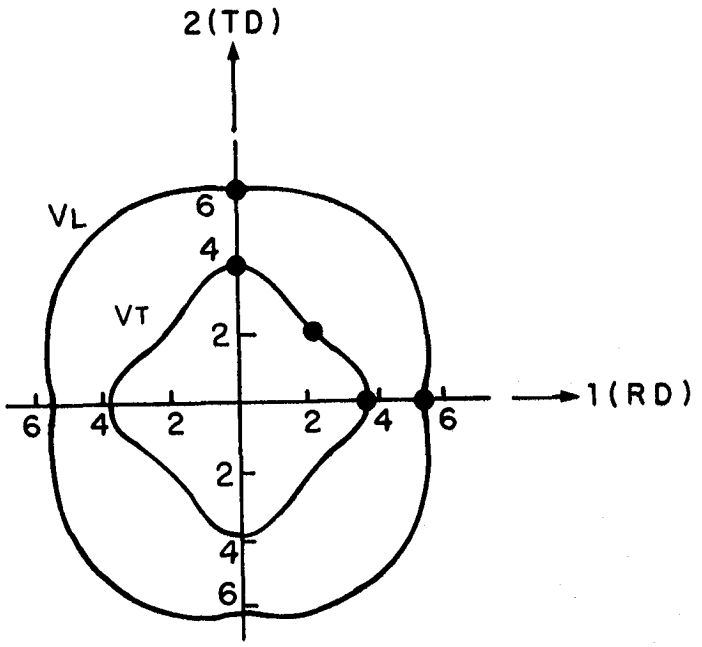

Fig. 6. Measurements required for nondestructive determination of stress and texture parameters. The solid lines schematically indicate the angular dependence of the velocities and the dots indicate the points at which data is required.

of the CODF as a means of correlating texture with mechanical properties has shown considerable recent promise (ref. 18), such a technique might be of considerable value in process control.

REFERENCES

1. J. F. Nye: Physical Properties of Crystals. Oxford, 1957.

2. Sayers, C. M. and Allen, D. R. J.: Phys. D., vol. 17, p. 1399.

3. B. A. Auld: Elastic Waves and Fields in Solids. Wiley, NY, 1973.

4. Thompson, R. B., Lee, S. S., and Smith, J. F.: Review of Progress in Quantitative Nondestructive Evaluation 3. D. O. Thompson and D. E. Chimenti, Eds., Plenum Press, NY, 1984, p. 1311.

5. Thompson, R. B., Smith, J. F., Lee, S. S.: Review of Progress in Quantitative Nondestructive Evaluation 2. D. O. Thompson and D. E. Chimenti, Eds., Plenum Press, NY, 1983, p. 1337.

6. Thompson, R. B., Smith, J. F., and Lee, S. S.: Appl. Phys. Lett., vol. 44, 1984, p. 296.

7. Thompson, R. B., Smith, J. F., and Lee, S. S.: Nondestructive Evaluation: Application to Materials Processing. O. Buck and S. M. Wolf, Eds., Amer. Soc. Metals, Metals Park, Ohio, 1984, p. 137.

8. Lee, S. S., Smith, J. F., and Thompson, R. B.: Evaluation of the Absolute Acoustoelastic Stress Measurement Technique. Review of Progress in Quantitative Nondestructive Evaluation 4, D. O. Thompson and D. E. Chimenti, Eds., Plenum Press, NY, (in press).

9. Liu, Y. C., and Alers, G. A.: Trans. Met. Soc. AIME, vol. 236, 1966, p. 489.

10. Papadakis, E. P.: Trans. Met. Soc. AIME, vol. 236, 1966, p. 1609.

11. Tittmann, B. R. and Alers, G. A.: Met. Trans., vol. 3, 1972, p. 1307.

12. Thompson, R. B. and Alers, G. A.: Proc. 9th Symposium on Nondestructive Evaluation. South Texas Section of ASNT and Southwest Research Institute, San Antonio, 1973, p. 6.

13. Thompson, R. B.: 1977 Ultrasonics Symposium Proceedings. IEEE, NY, 1977, p. 74.

14. Roe, R. J.: J. Appl. Phys., vol. 36, 1965, p. 2024.

15. Bunge, H. J.: Krist. Tech., vol. 3, 1968, p. 431.

16. Smith, J. F., Alers, G. A., Armstrong, P. E., and Eash, D. T.: Separation and Characterization of Stress Levels and Texture in Metal Sheet and Plate: I. Principles and Initial Test. To be published in J. Nondestructive Eval.

17. Droney, B. E.: Nondestructive Methods for Material Property Determination. C. O. Ruud and R. E. Green, Eds., Plenum Press, NY, 1984, p. 237.

18. Sowerby, R.: Deformation Textures in Some Non-Ferrous Metals. To be published in the proceedings of the symposium on texture of non-ferrous metals held as part of the 1984 Fall TMS-AIME Meeting, Sept. 16-20, 1984, Detroit, Michigan.